RSC Advances

PAPER

Cite this: *RSC Adv.*, 2022, **12**, 1682

Electrochemical detection of mercuric(II) ions in aqueous media using glassy carbon electrode modified with synthesized tribenzamides and silver nanoparticles†

Aalia Manzoor,[a] Tayyaba Kokab,[a] Anam Nawab,[a] Afzal Shah, *[a] Humaira Masood Siddiqi *[a] and Asma Iqbal[ab]

Received 21st November 2021
Accepted 4th January 2022

DOI: 10.1039/d1ra08517d

rsc.li/rsc-advances

This study reports the synthesis, characterization, and mercuric ion detection ability of novel tribenzamides having flexible and rigid moieties. *N*-{4-[2-(1,3-Benzoxazolyl)]phenyl}-3,5-*N*,*N*′-bis(4-alkyloxybenzoyl) benzamides (TBa-TBc) were synthesized from newly synthesized diamine, *N*-(1,3-benzoxazol-2-yl-phenyl)-3,5-diaminobenzamide (BODA) and *p*-alkoxybenzoic acids (*p*-ABA) by amidation reaction. Structural characterization of the synthesized compounds was done through spectroscopic techniques (FT-IR and NMR). The synthesized tribenzamides along with silver nanoparticles were used for modification of a glassy carbon electrode. Square wave anodic stripping voltammetry was carried out to test the performance of the modified electrode for mercuric ion detection. The designed sensor was found to demonstrate the qualities of sensitivity, selectivity, reproducibility and anti-interference ability. The sensing platform helped in detecting femtomolar concentrations of mercuric ions which are much below the level declared toxic by the World Health Organization.

1. Introduction

Mercury is extensively distributed in the environment (air, water, soil) and is a naturally occurring heavy metal. Because of its severe immunotoxic, neurotoxic and genotoxic effects, it is considered a global pollutant and a highly dangerous element by the Environmental Protection Agency (EPA).[1–3] The central nervous system, cardiovascular system, immune system, thyroid glands and kidneys are the recognized target organs. Mercury has been ranked as the 3rd most lethal element to humans by The United States (US) Government Agency for Toxic Substances and Disease Registry (ATSDR).[4] The prime form of mercury in its gaseous form is elemental mercury, also known as metallic mercury (Hg^0), having approximately six to twenty-four months atmospheric lifetime.[5] Elemental mercury (Hg^0) oxidizes readily to inorganic mercury (Hg^{2+}) and each form possesses different toxicity profiles and physicochemical properties.[6–8] European Commission and the EPA/FDA have threatened about the presence of mercury in food.[9,10] A global environmental treaty "the Minamata Convention on Mercury", came into force on August 16 2017 for monitoring mercury pollution to protect the human health as well as our surroundings from its hostile effects.[11]

The harmfulness of the compounds of mercury depends upon the exposure pathways.[12,13] To safeguard public health, the concentration of mercuric ions in drinking water must not exceed the threshold limit of 4.7 nM.[14] Therefore, precise identification and remediation of water toxins are extremely important for ensuring public safety.[15] Conventional techniques, including inductively coupled plasma mass spectrometry (ICPMS),[16,17] atomic fluorescence spectrometry (AFS)[18,19] and atomic absorption spectroscopy (AAS)[20] had been extensively used for mercury detection. Complicated sample treatment and expensive equipments are the practical limitations of these methods for *in situ* rapid analysis. Thus, there is an urgent need for cost affordable and ultrasensitive methods for monitoring mercury contamination.[21] In this regard electrochemical analyses are considered safer, faster and cheaper methods which could be exercised without complicated equipments. Among various electrochemical sensing techniques, SWASV is a prominent sensitive technique because of its fast speed of analysis, ease of operation and use of portable and inexpensive instrumentation.[22–24]

In order to satisfy the requirements of sensitivity, reusability and specificity lots of energies have been dedicated to the effective design of sensing systems for heavy metal ions.[25–28] To contribute in this domain, we used tribenzamides paired with silver nanoparticles as effective electrode modifier for mercuric

[a]*Department of Chemistry, Quaid-i-Azam University, Islamabad, 45320, Pakistan. E-mail: afzals_qau@yahoo.com; humairas@qau.edu.pk*

[b]*School of Chemistry and Chemical Engineering, State Key Laboratory of Metal Matrix Composites, Shanghai Jiao Tong University, Shanghai, 200240, P. R. China*

† Electronic supplementary information (ESI) available: ^{1}H NMR & ^{13}C NMR spectra of BODA, TBa, TBb, and TBc. See DOI: 10.1039/d1ra08517d

ions detection. Benzamides possess electrode-anchoring and metal ion complexing groups, thus act as a connecting medium and facilitator of electron transfer between the transducer (host) and mercuric ions (guest). The Ag NPs were used as a component of the modifier for enhancing conductivity of the electrode surface. Our designed sensing platform involving dual modifiers showed figures of merit in the context of stability, reproducibility and selectivity. Interestingly the modified electrode demonstrated excellent sensitivity as evidenced by the femtomolar detection of mercuric ions. This is because of the selective retention of the Hg^{2+} ions due to greater surface area of the modified electrode and greater affinity towards active hydrogen bearing amide functional group.[29–31] The mercury–amide interaction is an exception. It is remarkable to note that amides are the discriminating reagents for Hg^{2+} binding. This reaction is quite fast even at room temperature, whereas normally the amides are least reactive to the transition metal ions due to the amide nitrogen, which has reduced electron donating character. The mercury–amide linkage is covalent in nature.[32,33] The amide group is potentially distinctive for selective mercury binding from mixtures of ions.[34–37] Hence, spurred on by the mercury-amide linkage we synthesized tribenzamides and utilized them for mercuric ions sensor. The designed sensor helped in sensing mercuric ions present in water below the lower prohibited concentration limit set by the Environmental Protection Agency of USA.

2. Experimental design

2.1 Materials synthesis

Three different tribenzamides were synthesized by using the freshly prepared diamine (BODA) and three different *p*-alkyloxybenzoyl chlorides.

2.1.1 Synthesis of *N*-(1,3-benzoxazol-2-yl-phenyl)-3,5-diaminobenzamide (BODA). Novel diamine *N*-(1,3-benzoxazol-2-yl-phenyl)-3,5-diaminobenzamide (BODA) was synthesized by reducing the freshly prepared *N*-(1,3-benzoxazol-2-yl-phenyl)-3,5-dinitrobenzamide (BODN) according to reported procedure.[38] The general steps involved in the synthesis of diamine are presented in Scheme 1. Firstly, the dinitro compound was prepared by reacting 3,5-dinitrobenzoyl chloride and 2-(4-aminophenyl)benzoxazole. For which 3,5-dinitrobenzoic acid (10 g, 47 mmol) and $SOCl_2$ (7.2 mL, 61 mmol) were reacted for 8 hours to get 3,5-dinitrobenzoyl chloride. The unreacted $SOCl_2$ was recovered through vacuum distillation to get acid chloride. Solution of 2-(4-aminophenyl)benzoxazole (40 mmol) in dimethylacetamide (DMAc) was added dropwise to 3,5-dinitrobenzoyl chloride (40 mmol) at 0 °C through dropping funnel. Mixture was added in water after half an hour stirring of solution at r.t.[39] Filtration was done and product was washed with cold water. Recrystallization was done in ethanol.

In the second step, the synthesized dinitro benzamide was reduced to diamine for which ethanol (150 mL), 3,5-dinitrobenzamide (50 mmol), Pd/C (catalytic amount) and hydrazinium monohydrate 80% (300 mmol) were refluxed for 48 hours under nitrogen protection.[38] Pd/C was removed through filtration and the product was obtained by evaporation of ethanol. Ethanol was used for recrystallization of product.

BODN: yield: 81%, $R_f = 0.55$; melting point: 258–260 °C, IR: 3090 (C_{sp^2}–H str.), 3272 (N–H str.), 1681 (C=O str.), 1608 (C=C aromatic bend), 1530, 1314 (C–N str.), 1344 (N–O str.).

BODA: yield: 70% and mp 305–307 °C, $R_f = 0.40$; IR: 3460 (N–H amide stretch), 3358, 3330 (N–H amine stretch), 3272 (C_{sp^2}–H stretch), 1587 (C=C aromatic bend), 1645 (C=O stretch), 1319 (C–N stretch); ^{1}H NMR: 4.98 (4H, s, 8, 8′), 6.01 (1H, s, 7), 6.32 (2H, s, 6, 6′), 7.18 (2H, d, $J = 8.4$ Hz, 2, 2′), 7.65 (2H, d, $J = 8.3$ Hz, 1, 1′), 7.94 (2H, d, $J = 8.1$ Hz, 3, 3′), 8.09 (2H, d, $J = 8.2$ Hz, 4, 4′), 10.18 (1H, s, 5); ^{13}C NMR: 102.77 (C, 14, 14′), 111.58 (C, 1, 16), 119.05 (C, 4), 120.33 (C, 10, 10′), 122.01 (C, 2), 122.72 (C, 3), 125.22 (C, 8), 127.35 (C, 9, 9′), 135.48 (C, 11, 13), 141.62 (C, 5), 149.67 (C, 15, 15′), 151.72 (C, 6), 162.72 (C, 7), 168.00 (C, 12).

2.1.2 Synthesis of tribenzamides (*N*-{4-[2-(1,3-benzoxazolyl)]phenyl}-3,5-*N*,*N*′-bis(4-alkyloxybenzoyl)benzamide). This novel diamine was then utilized to synthesize three different tribenzamides (TBa, TBb, TBc) using three different *p*-alkyloxybenzoyl chlorides. The general steps are given in Scheme 2.

A mixture of thionyl chloride ($SOCl_2$) (8 mL) and *p*-alkoxybenzoic acid (40 mmol) was refluxed for 6 hours to get acid

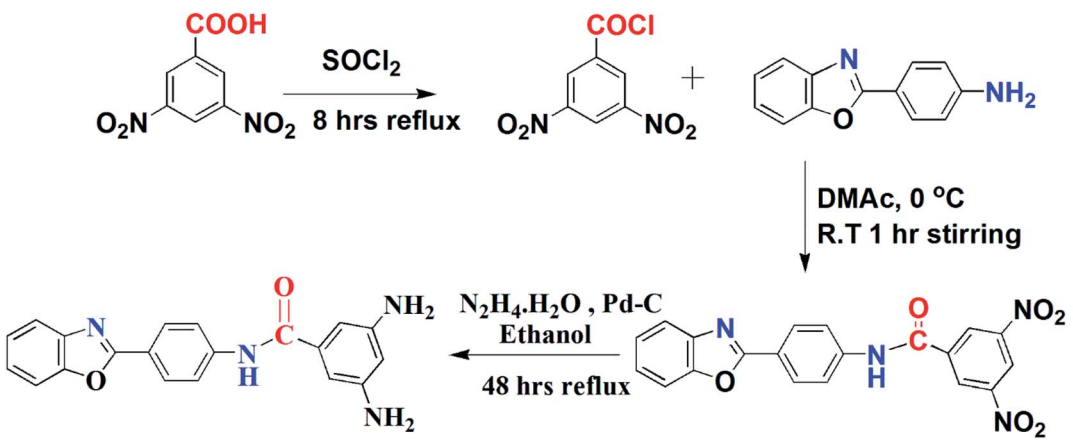

Scheme 1 Synthesis of *N*-(1,3-benzoxazol-2-yl-phenyl)-3,5-diaminobenzamide.

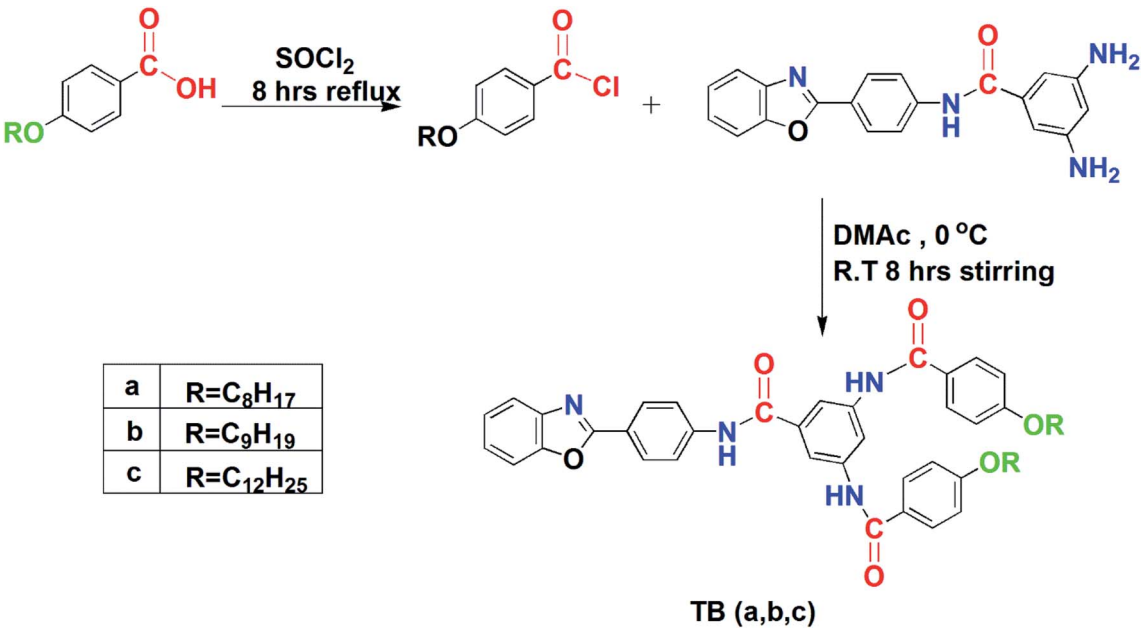

Scheme 2 Synthesis of tribenzamides [TB (a, b, c)].

chloride. 20 mmol solution of diamine in dimethylacetamide (DMAc) was added drop by drop to acid chloride through a dropping funnel at 0 °C and was stirred for eight hours at r.t. TLC (*n*-hexane : ethylacetate (1 : 4)) was done to monitor the reaction. Filtration was done to get the product after pouring the mixture into water. The product was washed with excess water. Repeated recrystallization was done in methanol, ethylacetate and THF respectively to ensure the purity.

2.1.2.1. N-{4-[2-(1,3-Benzoxazolyl)]phenyl}-3,5-N,N′-bis(4-octyloxybenzoyl)benzamide (TBa). R_f = 0.59, yield = 85%, mp 186–188 °C, IR: 3310 (N–H amide str.), 3016 (C_{sp^2}–H str.), 2914, 2874 (C_{sp^3}–H str.), 1675 (C=O str.), 1604 (C=C aromatic bend), 1240 (C–O stretch). ^{1}H NMR: 0.83 (6H, t, J = 6.9 Hz, 17, 17′), 1.26 (10H, m, 12, 12′–16, 16′), 1.69 (4H, quin, J = 6.6 Hz, 11, 11′), 4.02 (4H, t, J = 6.6 Hz, 10, 10′), 6.87 (4H, d, J = 8.2 Hz, 9, 9′), 7.07 (2H, d, J = 8.4 Hz, 2, 2′), 7.43 (2H, d, J = 8.0 Hz, 3, 3′), 7.74 (2H, d, J = 8.3 Hz, 1, 1′), 7.85 (4H, m, 4, 4′; 8, 8′), 8.00 (2H, s, 6, 6′), 8.26 (1H, s, 7), 10.69 (3H, s, 5, 5′, 5″); ^{13}C NMR: 14.42 (C, 28), 22.55 (C, 27), 25.91 (C, 26), 28.93 (C, 25), 29.05 (C, 24), 29.20 (C, 23), 31.70 (C, 22), 68.22 (C, 21), 110.08 (C, 1), 111.13 (C, 14, 14′), 114.53 (C, 19, 19′, 19″, 19‴), 114.66 (C, 16), 120.73 (C, 4), 121.54 (C, 10, 10′), 123.22 (C, 2), 124.03 (C, 3), 126.85 (C, 8, 17, 17′), 128.61 (C, 9, 9′), 130.17 (C, 13, 18, 18′, 18″), 131.79 (C, 11, 15, 15′), 140.14 (C, 5), 150.60 (C, 6), 161.99 (C, 20, 20′), 162.76 (C, 7), 167.47 (C, 12, 12′, 12″).

2.1.2.2. N-{4-[2-(1,3-Benzoxazolyl)]phenyl}-3,5-N,N′-bis(4-nonyloxybenzoyl)benzamide (TBb). R_f = 0.60, yield = 83%, mp 188–190 °C, IR: 3312 (N–H amide str.), 3020 (C_{sp^2}–H str.), 2915, 2865 (C_{sp^3}–H str.), 1675 (C=O str.), 1604 (C=C aromatic bend), 1242 (C–O stretch). ^{1}H NMR: 0.85 (6H, t, J = 6.8 Hz, 18, 18′), 1.24 (24H, m, 12, 12′–17, 17′), 1.68 (4H, quin, J = 6.6 Hz, 11, 11′), 4.01 (4H, t, J = 6.5 Hz, 10, 10′), 6.69 (4H, d, J = 8.1 Hz, 9, 9′), 7.04 (2H, d, J = 8.7 Hz, 2, 2′), 7.33 (2H, d, J = 8.2 Hz, 3, 3′), 7.68 (2H, d, J = 8.6 Hz, 1, 1′), 7.88 (4H, m, 4, 4′; 8, 8′), 8.02 (2H, s, 6, 6′), 8.21 (1H, s, 7), 10.67 (3H, s, 5, 5′, 5″); ^{13}C NMR: 14.40 (C, 29), 22.55 (C, 28), 25.89 (C, 27), 28.98 (C, 26), 29.11 (C, 25), 29.20 (C, 24), 29.41 (C, 23), 31.73 (C, 22), 68.21 (C, 21), 110.18 (C, 1), 111.23 (C, 14, 14′), 114.52 (C, 19, 19′, 19″, 19‴), 114.64 (C, 16), 120.37 (C, 4), 121.74 (C, 10, 10′), 123.22 (C, 2), 124.23 (C, 3), 126.86 (C, 8, 17, 17′), 128.10 (C, 9, 9′), 130.16 (C, 13, 18, 18′, 18″), 131.79 (C, 11, 15, 15′), 140.14 (C, 5), 150.60 (C, 6), 161.98 (C, 20, 20′), 162.78 (C, 7), 167.47 (C, 12, 12′, 12″).

2.1.2.3. N-{4-[2-(1,3-Benzoxazolyl)]phenyl}-3,5-N,N′-bis(4-dodecyloxybenzoyl)benzamide (TBc). R_f = 0.66, yield = 85%, mp 222–224 °C; IR: 3320 (N–H amide str.), 3050 (C_{sp^2}–H str.), 2918, 2876 (C_{sp^3}–H str.), 1681 (C=O str.), 1608 (C=C aromatic bend), 1250 (C–O stretch); ^{1}H NMR: 0.82 (6H, t, J = 6.8 Hz, 21, 21′), 1.22 (36H, m, 12, 12′–20, 20′), 1.71 (4H, quin, J = 6.6 Hz, 11,11′), 4.02 (4H, t, J = 6.7 Hz, 10, 10′), 6.66 (4H, d, J = 8.2 Hz, 9, 9′), 7.09 (2H, d, J = 8.5 Hz, 2, 2′), 7.41 (2H, d, J = 7.8 Hz, 3, 3′), 7.77 (2H, d, J = 8.4 Hz, 1, 1′), 7.87 (4H, m, 4, 4′, 8, 8′), 8.08 (2H, s, 6, 6′), 8.22 (1H, s, 7), 10.80 (3H, s, 5, 5′, 5″); ^{13}C NMR: 14.41 (C, 32, 32′), 22.57, 25.89, 28.98, 29.19, 29.49 (C, 23, 23′- 31, 31′), 31.77 (C, 22, 22′), 68.19 (C, 21, 21′), 110.23 (C, 1), 111.45 (C, 14, 14′), 114.62 (C, 19, 19′, 19″, 19‴), 115.78 (C, 16), 120.23 (C, 4), 121.45 (C, 10, 10′), 123.21 (C, 2), 124.56 (C, 3), 125.28 (C, 8, 17, 17′), 128.59 (C, 9, 9′), 130.32 (C, 13, 18, 18′, 18″), 131.78 (C, 11, 15, 15′), 142.15 (C, 5), 150.63 (C, 6), 161.98 (C, 20, 20′), 162.74 (C, 7), 167.45 (C, 12, 12′, 12″).

2.2 Physical measurements and instrumentation

The melting points of all the synthesized compounds were determined using open capillary tubes, on melting point apparatus, Mel-Temp, Mitamura Riken Kogyo, Inc. Tokyo Japan using open capillary tubes. Thermo Scientific Nicolet 6700 instrument was used to record the solid state ATR-FTIR spectra

(400–4000 cm^{-1}). NMR spectra (^1H and ^{13}C) were recorded on Bruker 300 MHz digital NMR instrument using deuterated DMSO as solvent. The spectra were calibrated with respect to the residual solvent signal. Metrohm Autolab PGSTAT302N running with NOVA 1.11 software was used for testing the efficiency of the designed sensor. The electrochemical cell consisted of bare and modified glassy carbon (GC) electrode, Ag/AgCl (3 M KCl) and Pt as working, reference and counter electrodes respectively.

The starting materials and reagents for synthesis, were purchased from Merck Germany and Sigma Aldrich and were used without purification unless otherwise stated. Solvents such as acetone, and dichloromethane (Merck) were distilled from CaH_2 whereas ethanol from CaO as drying agents and subsequently stored over 4 Å molecular sieves. Aluminium plates (0.2 mm thickness), precoated silica gel 60 F254 by E-Merck, and mixture of *n*-hexane : ethyl acetate as mobile phase were used for thin layer chromatography to monitor the reaction. Analytical grade mercuric chloride of 99% purity was used as analyte. Synthesis of silver nanoparticles was done according to the reported procedure by Afzal Shah and coworkers.[40] Britton Robinson (BR) buffer of pH 5, HNO_3, HCl, H_2SO_4, KOH, NaOH and KCl obtained from Sigma Aldrich were tested as supporting electrolytes. All solutions for electrochemical studies were prepared in doubly distilled water except dimethyl sulfoxide (DMSO) that helped dissolution of TBa for anchoring it over the electrode surface. Electrochemical experiments were conducted under deaerated conditions.

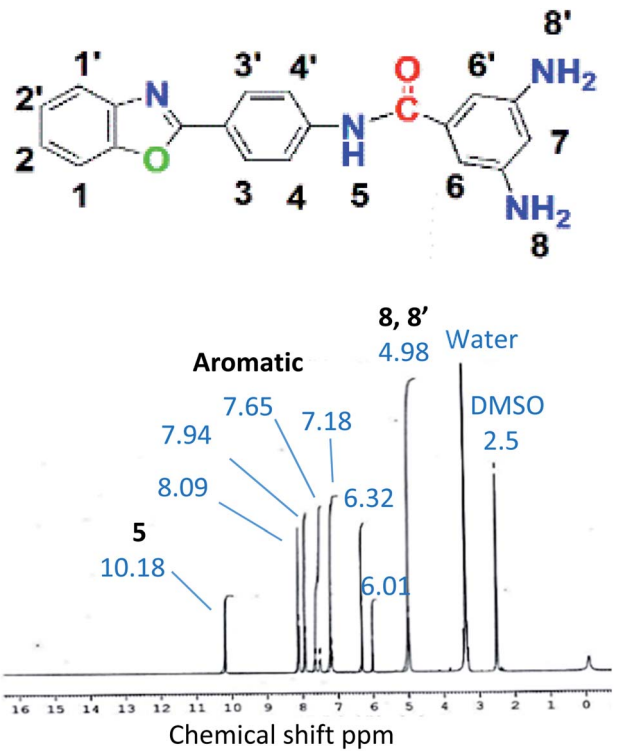

Fig. 1 ^1H NMR spectrum of BODA.

3. Results and discussion

3.1 Spectral analysis of the synthesized compounds

3.1.1 NMR analysis of diamine BODA. The ^1H NMR spectrum of the synthesized diamine (BODA) is given in Fig. 1. Four amino protons (8, 8′) appeared at 4.98 ppm. Proton 7, appeared at 6.01 ppm as is ortho to two amine groups whereas two protons (6, 6′) ortho to the carbonyl group resonated at 6.32 ppm. Two protons (2, 2′) resonated at 7.18 ppm, whereas 1, 1′ protons appeared at 7.65 ppm as they are ortho to the heteroatom. Signal at 7.94 ppm was assigned to 3, 3′ protons and a comparatively deshielded signal at 8.09 ppm was attributed to 4, 4′ protons, ortho to amide group. The amide proton 5 appeared as the most deshielded proton at 10.18 ppm. Successful synthesis of BODA was confirmed through this pattern.

3.1.2 ^1H NMR analysis of tribenzamide (TBa). In ^1H NMR of TBa given in Fig. 2. 6 protons (17, 17′) appeared at 0.83 ppm as triplet. 20 protons (12, 12′–16, 16′) resonated as multiplet at 1.26 ppm and four protons (10, 10′) resonated as a triplet at 4.02 ppm. Aromatic protons resonated at their particular region. Proton (7) appeared at 8.22 ppm as singlet and a comparatively deshielded singlet at 10.80 ppm was attributed to three amide protons (5, 5′, 5″). Successful synthesis of TBa was confirmed through this NMR pattern.

3.2 Mercuric ions detection

3.2.1 Electrode pretreatment and modification of GCE. Before modification of the GCE with the recognition layer, its surface pretreatment was performed both physically and electrochemically. During physical pretreatment, the GCE surface was polished manually with a slurry of diamond powder (1 μm particle size) on a polishing pad followed by ultra-sonication to remove attached slurry particles. Then it was rinsed thoroughly with doubly distilled water. After this step electrochemical precleaning was performed to obtain a reproducible surface, by applying ten repeated cyclic voltammograms between −1.4 V and +0.9 V in phosphate buffer at 100 mV s^{-1}, resulting in the achievement of a stable polarization cycle. This pretreated GCE was then drop casted with 5 μL volume of 30 μM TBa solution, followed by the evaporation of solvent *via* hot air drying method. The square wave adsorptive stripping voltammetry (SWASV) was then applied using modified GCE for the sensing of mercury(II). Influence of Ag nanoparticles (NPs) on the electrocatalytic role of TBa modified electrode was also investigated. For this purpose tribenzamide (TBa) coated GCE was kept in the suspension of Ag NPs for 30 min. Then it was dried under inert conditions by flushing a stream of argon. The performance of the resulting electrode symbolized by TBa/Ag NPs/GCE was used for the analytical determination of mercuric ions under optimized conditions. Nitrogen gas was purged for 10 minutes through all the solutions before starting an electrochemical experiment to avoid the appearance of oxygen signals in the voltammograms. The deposition step of the SWASV technique leading to the electroplating of Hg^{2+} ions onto the GCE surface was carried out under predefined deposition potential of −1.2 V

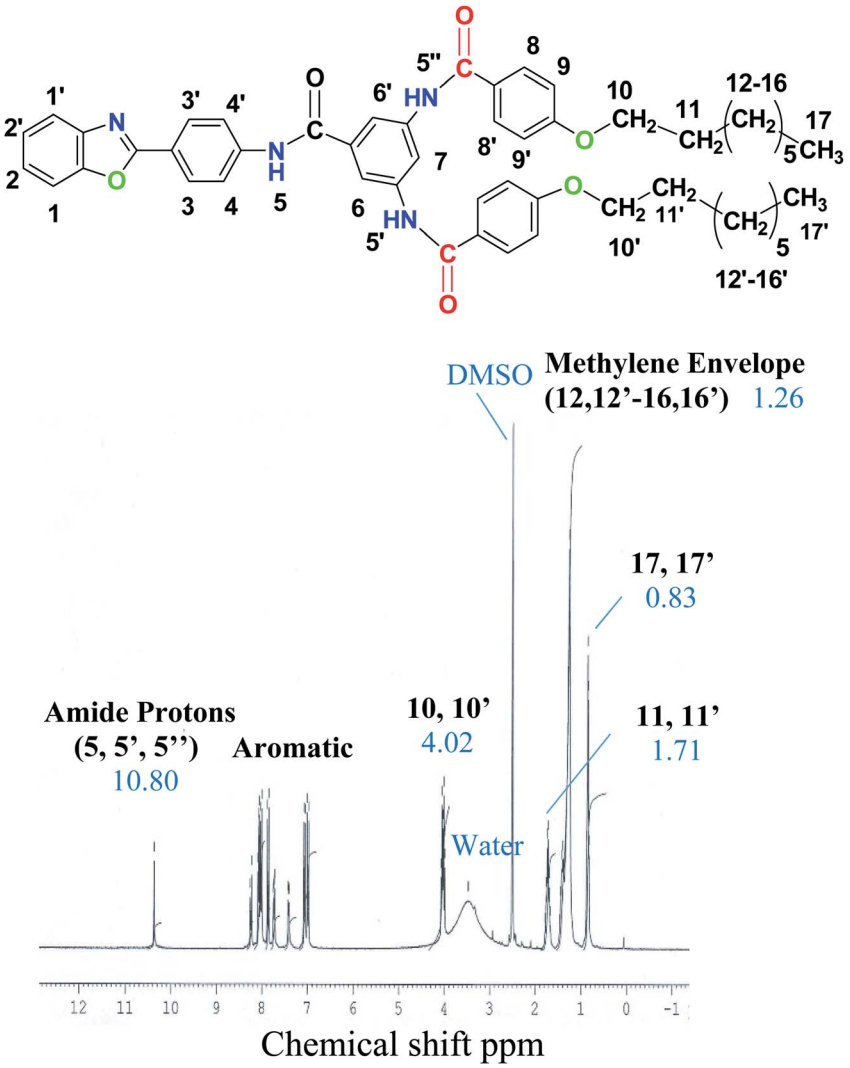

Fig. 2 ^{1}H NMR spectrum of TBa.

during 100 s. The stripping step of SWASV caused the oxidation of the electroplated atoms during scanning of the potential towards positive values. Modified electrode surface was freshly prepared for each electrochemical experiment.

3.2.2 Selection of the best electrode modifier. The voltammetric response of tribenzamide (TBa) modified electrode was first tested by cyclic voltammetry (CV) in 1 mM $HgCl_2$ solution using Britton Robinson (BR) buffer of pH-5 as supporting electrolyte. CV results showed the lowest intensity of peak current at bare GCE (Fig. 3a). While TBa modified electrode led to signal intensification. Silver nanoparticles coated over TBa modified GCE further enhanced the sensitivity of the designed sensor as demonstrated in Fig. 3b and c. This enhancement can be related to the role of Ag NPs in providing more active sites at the electrode surface for accumulation of Hg^{2+} ions. The more intense CV signals on dual modification of GCE specify that benzamide molecules offer electron donor groups for mercuric ions interactions on electrode surface while Ag NPs enhance electrode surface area as well as conductivity. Moreover, dual modification of GCE not only significantly improves sensitivity but also causes splitting of the two steps, one electron oxidation processes of Hg^{0} to Hg^{2+} as verified by the appearance of two anodic signals in the cyclic voltammograms. Thus, cyclic voltammograms present that TBa/Ag NPs/GCE is able to detect both Hg^{1+} and Hg^{2+} ions.

3.2.3 Conditions optimization. The experimental conditions including pH of medium, stripping solvent, deposition potential and deposition time were optimized to get the highest peak current response at both modified electrodes (TBa modified GCE and TBa/Ag NPs/GCE).

The pH of the medium controls the electrode surface reactions and protons/analyte ions availability in solution. SWASV of Hg^{2+} solution at the designed sensors was carried out in BRB solutions of different pH ranging from 2 to 9. The best response for mercuric ions sensing was observed in media of acidic pH as shown in Fig. 4A and B. Mercury exists as Hg^{2+} in acidic pH while in solutions of basic pH, it precipitates out as insoluble $Hg(OH)_2$. This complexation in alkaline medium leads to weak

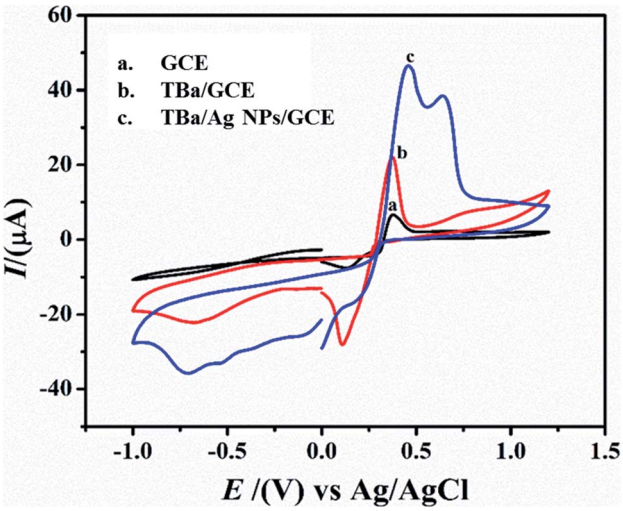

Fig. 3 Cyclic voltammograms of 1 mM $HgCl_2$ obtained at bare GCE (a), modified GCE with TBa (b) and modified GCE with TBa and silver nanoparticles (c) in BRB of pH 5 at a scan rate of 100 mV s^{-1}.

signals as observed in solutions of pH higher than 7. An observation of the SWASV of 1 mM Hg^{2+} solution recorded at the designed sensors in solutions of BRB (pH-2), 0.1 M HNO_3, 0.1 M HCl, 0.1 M H_2SO_4, 0.1 M KOH, 0.1 M NaOH and 0.1 M KCl (Fig. 5A and B) reveals that among the tested supporting electrolytes the highest peak intensity and better peak shape of the oxidation of electroreduced mercuric ions appear in HCl solution. So, subsequent electroanalytical experiments for mercuric ions detection were conducted in solutions with HCl as supporting electrolyte.

The deposition of metal ions at the surface of electrode are required for effective stripping study of metals. The deposition step determines the optimum loading of metal ions onto the electrode surface resulting from applied deposition potential and deposition time. Therefore, SWAS voltammetry was conducted by changing the deposition potential from 0 V to −1.5 V at both TBa modified GCE and TBa/Ag NPs/GCE as shown in Fig. 6. The peak current enhanced with deposition potential from −0.2 V to −1.2 V because of efficient electroreduction of metal ions at more negative potentials. However, on application of further higher potentials, *i.e.*, from −1.2 V to −1.5 V, peak current decrement occurred possibly due to water splitting which occurs in this potential domain. Hence, based upon the maximum stripping current intensity at −1.2 V, the influence of deposition time was examined at optimized deposition potential of −1.2 V as shown in Fig. 7. The highest peak current response was noticed at deposition time of 100 s whereas longer deposition time led to diminution in current signals which could be attributed to multilayer formation of the modifier with expected lower accessibility of target metal ions.

3.3 Analytical determination

The optimized conditions were practiced for the electroanalytical detection of Hg^{2+} ions at both TBa modified GCE and TBa coated silver nanoparticles modified GCE, independently. The SWAS voltammograms of mercuric ions as displayed in Fig. 8 were recorded by successive dilutions of the concentration of mercuric ions at TBa/GCE and at TBa/Ag NPs/GCE. The trace level detection limits up to femtomolar concentration of Hg^{2+} ions at our designed electrochemical platform is compared with the sensing performance of the reported sensors[41–51] as listed in Table 1. A comparison of the tabulated values reveals that our designed sensor is a preferred analytical tool for mercuric ions detection.

3.4 Interference effect

To assess the discrimination capability of the sensor, the signal of the target analyte was investigated in the presence of inorganic and organic interfering agents. The electrochemical signal of Hg^{2+} ions in the presence of 2 mM concentrations of each interfering species under optimized conditions was

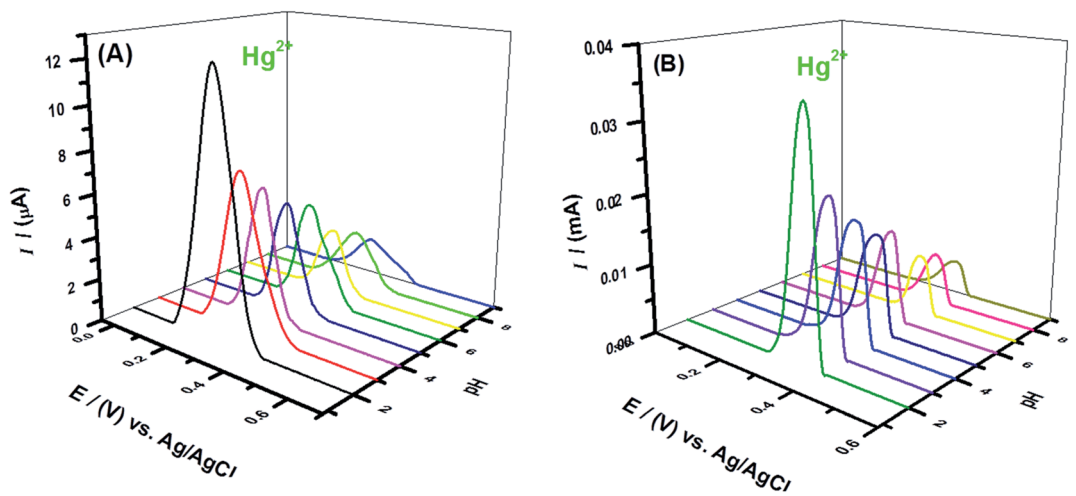

Fig. 4 SWASV showing the effect of various pH values on the peak current of 1 mM Hg^{2+} solution using (A) TBa modified GCE (B) TBa/Ag NPs/GCE using SWASV at a scan rate of 100 mV s^{-1} and setting deposition potential of −1.2 V.

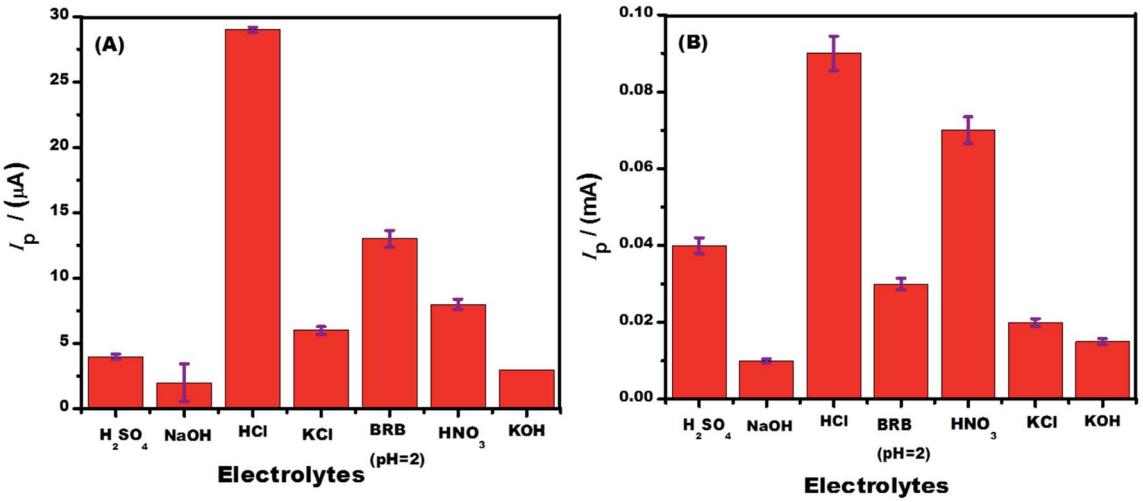

Fig. 5 Bar graphs showing the effect of various electrolytes on the peak current of 1 mM Hg^{2+} solution using (A) TBa modified GCE (B) TBa/Ag NPs/GCE using SWASV at a scan rate of 100 mV s^{-1} and setting deposition potential of −1.2 V.

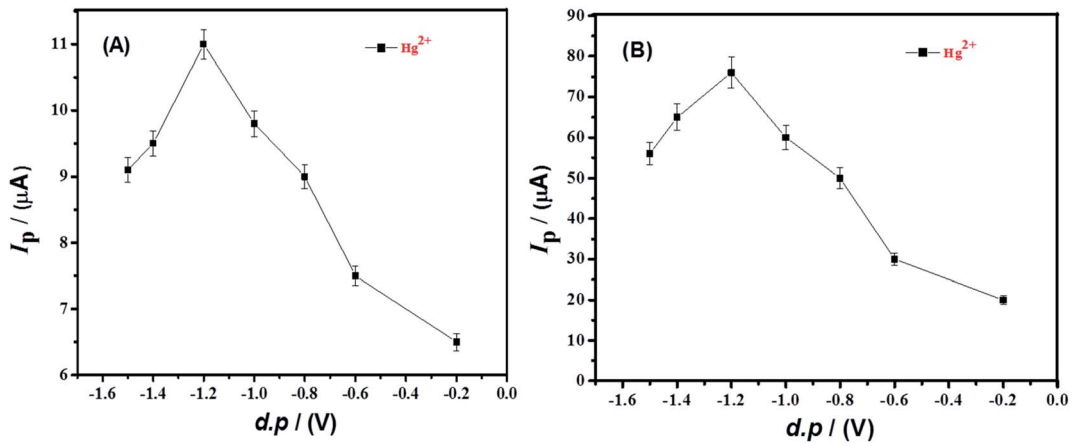

Fig. 6 Peak current of 0.5 mM Hg^{2+} solution in HCl as a function of deposition potential using data obtained from SWASV carried out at a scan rate of 100 mV s^{-1} at (A) TBa/GCE and (B) TBa/Ag NPs/GCE.

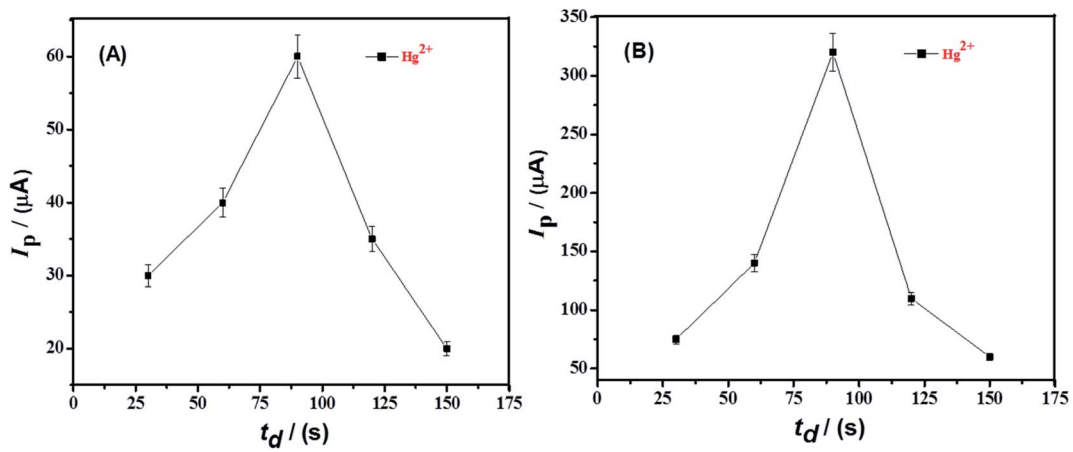

Fig. 7 Deposition time impact on the oxidation peak current of 1 mM Hg^{2+} solution possessing HCl as supporting electrolyte using data obtained from SWASV carried out at (A) TBa/GCE and (B) TBa/Ag NPs/GCE under conditions of 100 mV s^{-1} scan rate and deposition potential of −1.2 V.

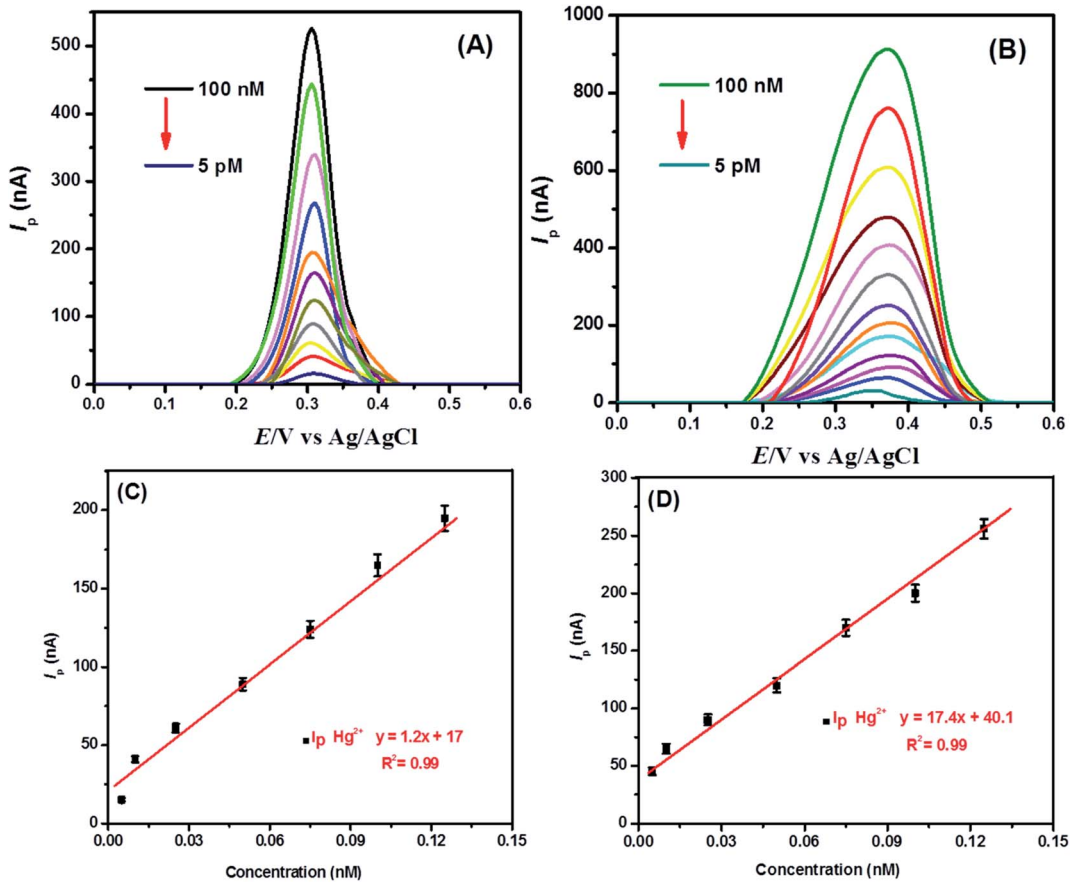

Fig. 8 SWASV recorded over the surface of (A) TBa/GCE and (B) TBa/Ag NPs/GCE under optimized conditions in aqueous solutions containing varying concentration of Hg^{2+} using HCl as supporting electrolyte (C & D) calibration plots.

Table 1 Comparison of the detection of Hg^{2+} ions at various modified electrodes

Electrode substrate[a]	Measurement technique	LOD (M)	Reference
MWCNTs/IL/CPE	Potentiometry	2.5×10^{-9}	41
AuNPs–GO-IL/GCE	SWASV	3.0×10^{-11}	42
AuNPs-GCE	SWASV	19.0×10^{-12}	43
IIP-CILE	DPASV	0.1×10^{-9}	44
PPE-GCE	SWASV	0.1×10^{-9}	45
IIP–MWCNTs-GCE	DPASV	5.0×10^{-9}	46
HMSN-CPE	SWASV	2.3×10^{-8}	47
NGME	DPSV	50.0×10^{-9}	48
IAP30/RTIL electrode	SWSV	6.0×10^{-11}	49
GO-AuNPs/MTU modified ITO	DPASV	7.8×10^{-10}	50
SnO_2/RGO nanocomposite/GCE	SWASV	2.8×10^{-10}	51
TBa modified GCE	SWASV	25×10^{-15}	This work
TBa/Ag NPs/GCE	SWASV	1.7×10^{-15}	This work

[a] MWCNTs/IL/CPE = multi-walled carbon nanotubes-ionic liquid-carbon paste electrode; AuNPs–GO-IL/GCE = graphene oxide-ionic liquid composites–gold nanoparticle; AuNPs-GCE = gold nanoparticle-modified glassy carbon electrode; IIP-CILE = carbon ionic liquid paste electrode impregnated with novel ion imprinted polymeric nanobeads; PPE = 1-phenyl-*N*-(pyridin-2-ylmethyl)ethanamin; IIP–MWCNTs-GCE = imprinted polymeric nanobeads and multi-wall carbon nanotubes; HMSN-CPE = carbon paste electrode modified with hybrid mesostructured silica nanoparticles; NGME = N-doped graphene modified electrode; IAP30/RTIL electrode = irradiated attapulgite/ionic liquid composites; GO-AuNPs/MTU modified ITO = ITO electrode modified with 5-methyl-2-thiouracil, graphene oxide and gold nanoparticles; SnO_2/RGO nanocomposite = SnO_2/reduced graphene oxide nanocomposite.

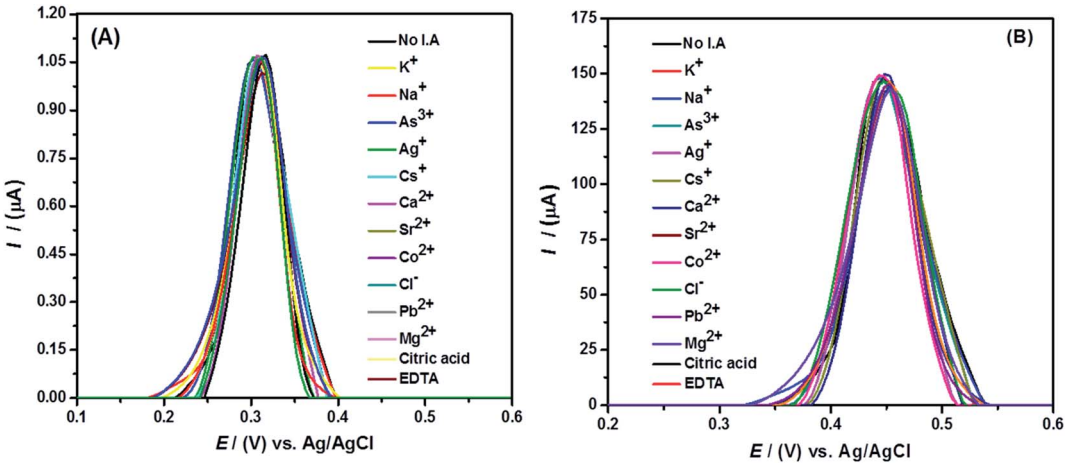

Fig. 9 SWASV recorded over the surface of (A) TBa/GCE and (B) TBa/Ag NPs/GCE under optimized conditions in aqueous solutions containing 100 μM concentration of Hg^{2+} with 2 mM concentration of each interfering agent using HCl as supporting electrolyte.

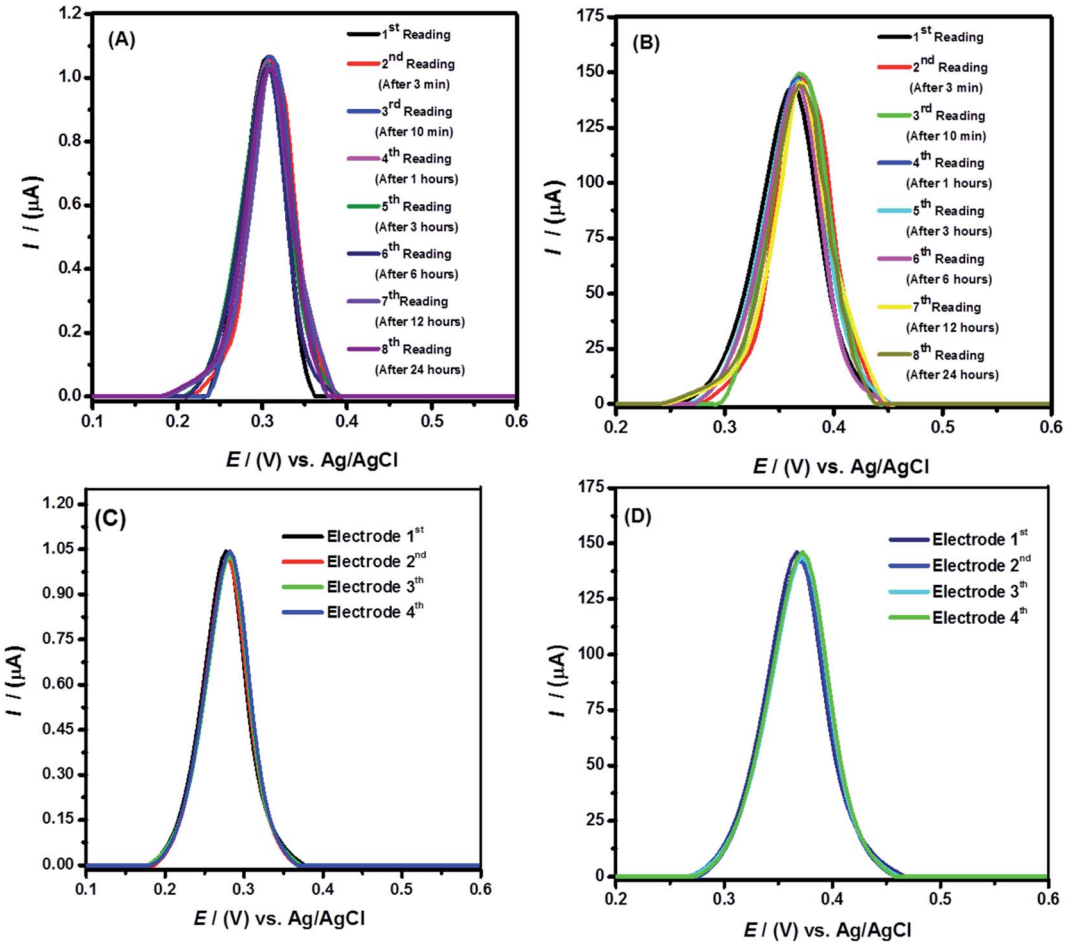

Fig. 10 The SWASV of 100 μM Hg^{2+} solutions under optimized conditions; (A) showing repeatability ($n = 8$) of the TBa/GCE (B) TBa/Ag NPs/GCE (C) showing reproducibility of multiple electrodes ($n = 4$) modified by TBa/GCE and (D) TBa/Ag NPs/GCE under optimized conditions.

obtained as shown in Fig. 9. The peak current of Hg^{2+} ions with a percent relative standard deviation (% RSD) of less than 3% reveals strong anti-interference ability of the designed sensing platform.

3.5 Repeatability and reproducibility

The repeatability, stability and reliability of the sensor were assessed by recording eight consecutive voltammograms at the same modified electrode under similar conditions at different

Table 2 Results for Hg^{2+} ions determination in real water samples using TBa/Ag NPs/GCE under optimized conditions

Sample	Initially found (nM)	Spiked amount (nM)	Found amount (nM)	Recovery (%)	RSD (%)
Drinking water 1	0.0	0.05	0.049 ± 0.002	98.0	2.3
Drinking water 2	0.0	0.05	0.047 ± 0.005	95.0	2.2
Tap water 1	0.0	0.05	0.048 ± 0.002	96.0	3.0
Tap water 2	0.0	0.05	0.048 ± 0.002	96.0	2.8
Spring water 1	0.0	0.05	0.049 ± 0.003	98.0	3.2
Spring water 2	0.0	0.05	0.048 ± 0.001	96.0	1.3

time intervals. The obtained SWV having % RSD < 2.5% display no significant difference in the signals of Hg^{2+} ions (see Fig. 10). Thus, SWV data for stability analysis present accuracy of the sensor's performance. Likewise, to check reproducibility of the sensor four electrodes were modified and used for Hg^{2+} ions detection. The identical voltammograms as shown in Fig. 10(C and D) point to the reproducibility of the designed sensing platform with % RSD < 2. Hence, the robust repeatability and reproducibility of the engineered sensor related to the retainment of modifier's integrity owing to its insolubility in aqueous media, confirm it as a promising tool for accurate analysis.

3.6 Real samples analysis

To explore the accuracy and practical applicability of the proposed methodology, the sensor was operated for real ecological samples analysis. However, initially no amount of Hg^{2+} was found in drinking and tap water samples. Then, recovery tests were performed by standard addition method under predefined conditions. The percentage recoveries in range of 95–100% (Table 2) verify validity of the designed sensor for practical applications.

4. Conclusion

In this work synthesis, characterization and mercuric ions detection ability of novel *N*-{4-[2-(1,3-benzoxazolyl)]phenyl}-3,5-*N*,*N*′-bis(4-alkyloxybenzoyl)benzamides (TBa-TBc) are presented. These compounds were characterized by spectroscopic techniques (FT-IR, ^{1}H and ^{13}C-NMR). Of the three tested compounds, best results were produced by TBa. The current study introduces TBa and TBa–silver nanoparticles as novel recognition elements of the GCE surface to improve its detection ability up to femtomolar concentration of mercuric ions. The results revealed a dramatic boost in the current response of mercury at the modified electrode surface compared to bare glassy carbon electrode. The detectability of the sensor was found much better than the reported sensors. Hence, our designed sensing platform holds great promise for the development of a practically viable water purification device owing to its peculiar features of simplicity, stability, anti-interference ability, ultra-sensitivity and practical applicability.

It is important to note that TBa-TBc are rare examples of organic mercuric ions detectors in water, which contain tribenzamide linkages, so other experiments are under active investigation.

Conflicts of interest

Authors declare no conflicts of interest.

Acknowledgements

The authors gratefully acknowledge the financial support of Higher Education Commission and Quaid-i-Azam University Islamabad, Pakistan.

References

1 D. Zhang, L. Wang, H. Zeng, P. Yan, J. Nie, V. K. Sharma and C. Wang, A three-dimensional macroporous network structured chitosan/cellulose biocomposite sponge for rapid and selective removal of mercury(II) ions from aqueous solution, *Chem. Eng. J.*, 2019, **363**, 192–202.

2 E. G. Pacyna, J. M. Pacyna, K. Sundseth, J. Munthe, K. Kindbom, S. Wilson and P. Maxson, Global emission of mercury to the atmosphere from anthropogenic sources in 2005 and projections to 2020, *Atmos. Environ.*, 2010, **44**, 2487–2499.

3 J. Wang and X. Qian, A series of polyamide receptor based PET fluorescent sensor molecules: positively cooperative Hg^{2+} ion binding with high sensitivity, *Org. Lett.*, 2006, **8**, 3721–3724.

4 L. T. Budnik and L. Casteleyn, Mercury pollution in modern times and its socio-medical consequences, *Sci. Total Environ.*, 2019, **654**, 720–734.

5 P. Holmes, K. A. F. James and L. S. Levy, Is low-level environmental mercury exposure of concern to human health?, *Sci. Total Environ.*, 2009, **408**, 171–182.

6 L. R. Goldman, M. W. Shannon and Committee on Environmental Health, Technical report: mercury in the environment: implications for pediatricians, *Pediatrics*, 2001, **108**, 197–205.

7 W. Crowe, P. J. Allsopp, G. E. Watson, P. J. Magee, J. J. Strain, D. J. Armstrong and E. M. McSorley, Mercury as an environmental stimulus in the development of autoimmunity – a systematic review, *Autoimmun. Rev.*, 2017, **16**, 72–80.

8 B. Braune, J. Chételat, M. Amyot, T. Brown, M. Clayden, M. Evans and G. Stern, Mercury in the marine environment of the Canadian Arctic: review of recent findings, *Sci. Total Environ.*, 2015, **509**, 67–90.

9 https://www.epa.gov/fish-tech/epa-fda-fish-advice-technical-information, 2018.

10 https://ec.europa.eu/food/safety/chemical_safety/contaminants/catalogue/mercury-en, 2018.

11 http://www.mercuryconvention.org/Resources/Information/tabid/5137/language/en-US/Default.aspx, 2018.

12 F. Ruggieri, C. Majorani, F. Domanico and A. Alimonti, Mercury in children: current state on exposure through human biomonitoring studies, *Int. J. Environ. Res. Public Health*, 2017, **14**, 519.

13 A. H. Stern, A review of the studies of the cardiovascular health effects of methylmercury with consideration of their suitability for risk assessment, *Environ. Res.*, 2005, **98**, 133–142.

14 A. Munir, A. Shah and B. Piro, Development of a selective electrochemical sensing platform for the simultaneous detection of Tl^{+}, Cu^{2+}, Hg^{2+}, and Zn^{2+} ions, *J. Electrochem. Soc.*, 2018, **165**, 399.

15 H. B. Sonmez and N. Bicak, Quaternization of poly(4-vinyl pyridine) beads with 2-chloroacetamide for selective mercury extraction, *React. Funct. Polym.*, 2002, **51**, 55–60.

16 Q. Liang, H. Jing and D. C. Gregoire, Determination of trace elements in granites by inductively coupled plasma mass spectrometry, *Talanta*, 2000, **51**, 507–513.

17 D. Beauchemin, Inductively coupled plasma mass spectrometry, *Anal. Chem.*, 2008, **80**, 4455–4486.

18 T. S. West, Atomic-fluorescence and atomic-absorption spectrometry for chemical analysis, *Analyst*, 1974, **99**, 886–899.

19 M. L. Chen, H. J. Ma, S. Q. Zhang and J. H. Wang, Mercury speciation with L-cysteine functionalized cellulose fibre as adsorbent by atomic fluorescence spectrometry, *J. Anal. At. Spectrom.*, 2011, **26**, 613–617.

20 O. T. Butler, W. R. L. Cairns, J. M. Cook and C. M. Davidson, Atomic spectrometry update. Environmental analysis, *J. Anal. At. Spectrom.*, 2010, **25**, 103–141.

21 Q. Lin, X. M. Jiang, X. Q. Ma, J. Liu, H. Yao, Y. M. Zhang and T. B. Wei, Novel bispillar [5] arene-based AIEgen and its' application in mercury(II) detection, *Sens. Actuators, B*, 2018, **272**, 139–145.

22 H. Li, J. Li, Z. Yang, Q. Xu, C. Hou, J. Peng and X. Hu, Simultaneous determination of ultratrace lead and cadmium by square wave stripping voltammetry with *in situ* depositing bismuth at Nafion-medical stone doped disposable electrode, *J. Hazard. Mater.*, 2011, **191**, 26–31.

23 Y. Zhang, Y. Liu, X. Ji, C. E. Banks and W. Zhang, Sea cucumber-like hydroxyapatite: cation exchange membrane-assisted synthesis and its application in ultra-sensitive heavy metal detection, *Chem. Commun.*, 2011, **47**, 4126–4128.

24 M. P. N. Bui, J. Brockgreitens, S. Ahmed and A. Abbas, Dual detection of nitrate and mercury in water using disposable electrochemical sensors, *Biosens. Bioelectron.*, 2016, **85**, 280–286.

25 S. Ruan, H. Ebendorff-Heidepriem and Y. Ruan, Optical fibre turn-on sensor for the detection of mercury based on immobilized fluorophore, *Measurement*, 2018, **121**, 122–126.

26 M. A. Abbasi, M. I. Aziz-ur-Rehman, S. Z. Siddiqui and M. Ashraf, Synthesis and pharmacological activities of *N*-(3-Hydroxyphenyl)Benzamide and its 3-O-derivatives, *Pak. J. Chem.*, 2014, **4**, 26–30.

27 K. Ramesh, S. N. Murthy, K. Karnakar, K. H. V. Reddy, Y. V. D. Nageswar, M. Vijay and R. B. N. Prasad, A mild and expeditious synthesis of amides from aldehydes using bio glycerol-based carbon as a recyclable catalyst, *Tetrahedron Lett.*, 2012, **53**, 2636–2638.

28 M. Sharif and X. F. Wu, Palladium-catalyzed synthesis of primary benzamides from aryl bromides *via* a cyanation and hydration sequence, *RSC Adv.*, 2015, **5**, 21001–21004.

29 S. Yoon, A. E. Albers, A. P. Wong and C. J. Chang, Screening mercury levels in fish with a selective fluorescent chemosensor, *J. Am. Chem. Soc.*, 2005, **127**, 16030–16031.

30 S. Yoon, A. E. Albers, A. P. Wong and C. J. Chang, Screening mercury levels in fish with a selective fluorescent chemosensor, *J. Am. Chem. Soc.*, 2005, **127**, 16030–16031.

31 S. Chiarle, M. Ratto and M. Rovatti, Mercury removal from water by ion exchange resins adsorption, *Water Res.*, 2000, **34**, 2971–2978.

32 E. Yavuz, B. F. Senkal and N. Bicak, Poly(acrylamide) grafts on spherical polyvinyl pyridine resin for removal of mercury from aqueous solutions, *React. Funct. Polym.*, 2005, **65**, 121–125.

33 J. Wang and X. Qian, A series of polyamide receptor based PET fluorescent sensor molecules: positively cooperative Hg^{2+} ion binding with high sensitivity, *Org. Lett.*, 2006, **8**, 3721–3724.

34 N. Biçak, D. C. Sherrington and B. F. Senkal, Graft copolymer of acrylamide onto cellulose as mercury selective sorbent, *React. Funct. Polym.*, 1999, **41**, 69–76.

35 B. F. Senkal and E. Yavuz, Ureasulfonamide polymeric sorbent for selective mercury extraction, *Monatsh. Chem.*, 2006, **137**, 929–934.

36 S. Mahesh, K. C. Tang and M. Raj, Amide bond activation of biological molecules, *Molecules*, 2018, **23**, 2615.

37 D. S. Ştefan, I. Untea, V. Neagu, C. Luca and M. Ştefan, Selective retention of Hg^{2+} ions from aqueous solutions by various amide groups-functionalized copolymers, *Rev. Roum. Chim.*, 2008, **53**, 617–622.

38 J. W. Larsen, M. Freund, K. Y. Kim, M. Sidovar and J. L. Stuart, Mechanism of the carbon catalyzed reduction of nitrobenzene by hydrazine, *Carbon*, 2000, **38**, 655–661.

39 H. Khani, M. K. Rofouei, P. Arab, V. K. Gupta and Z. Vafaei, Multi-walled carbon nanotubes-ionic liquid-carbon paste electrode as a super selectivity sensor: application to potentiometric monitoring of mercury ion(II), *J. Hazard. Mater.*, 2010, **183**, 402–409.

40 A. Shah, M. S. Malik, A. Zahid, F. J. Iftikhar, A. Anwar, M. S. Akhter and A. H. Shah, Carbamazepine coated silver nanoparticles for the simultaneous electrochemical sensing of specific food toxins, *Electrochim. Acta*, 2018, **274**, 131–142.

41 H. Khani, M. K. Rofouei, P. Arab, V. K. Gupta and Z. Vafaei, Multi-walled carbon nanotubes-ionic liquid-carbon paste electrode as a super selectivity sensor: application to

potentiometric monitoring of mercury ion(II), *J. Hazard. Mater.*, 2010, **183**, 402–409.

42 N. Zhou, J. Li, H. Chen, C. Liao and L. Chen, A functional graphene oxide-ionic liquid composites–gold nanoparticle sensing platform for ultrasensitive electrochemical detection of Hg^{2+}, *Analyst*, 2013, **138**, 1091–1097.

43 L. Laffont, T. Hezard, P. Gros, L. E. Heimbürger, J. E. Sonke, P. Behra and D. Evrard, Mercury(II) trace detection by a gold nanoparticle-modified glassy carbon electrode using square-wave anodic stripping voltammetry including a chloride desorption step, *Talanta*, 2015, **141**, 26–32.

44 A. Bahrami, A. Besharati-Seidani, A. Abbaspour and M. Shamsipur, A highly selective voltammetric sensor for nanomolar detection of mercury ions using a carbon ionic liquid paste electrode impregnated with novel ion imprinted polymeric nanobeads, *Mater. Sci. Eng., C*, 2015, **48**, 205–212.

45 A. Shah, S. Sultan, A. Zahid, S. Aftab, J. Nisar, S. Nayab and S. A. Ozkan, Highly sensitive and selective electrochemical sensor for the trace level detection of mercury and cadmium, *Electrochim. Acta*, 2017, **258**, 1397–1403.

46 H. R. Rajabi, M. Roushani and M. Shamsipur, Development of a highly selective voltammetric sensor for nanomolar detection of mercury ions using glassy carbon electrode modified with a novel ion imprinted polymeric nanobeads and multi-wall carbon nanotubes, *J. Electroanal. Chem.*, 2013, **693**, 16–22.

47 A. Sánchez, S. Morante-Zarcero, D. Pérez-Quintanilla, I. Sierra and I. del Hierro, Determination of Hg(II) in natural waters using a carbon paste electrode modified with hybrid mesostructured silica nanoparticles, *Sens. Actuators, B*, 2012, **163**, 38–43.

48 H. Xing, J. Xu, X. Zhu, X. Duan, L. Lu, W. Wang and T. Yang, Highly sensitive simultaneous determination of cadmium(II), lead(II), copper(II), and mercury(II) ions on N-doped graphene modified electrode, *J. Electroanal. Chem.*, 2016, **760**, 52–58.

49 S. Xiong, J. Xu, F. Xie, X. Hu, G. Gong, Z. Wu and L. Yao, Stripping analysis of Pb(II), Cd(II), Hg(II) and Cu(II) based on irradiated attapulgite/Ionic liquid composites, *Chem. Eng. J.*, 2017, **316**, 383–392.

50 N. Zhou, H. Chen, J. Li and L. Chen, Highly sensitive and selective voltammetric detection of mercury(II) using an ITO electrode modified with 5-methyl-2-thiouracil, graphene oxide and gold nanoparticles, *Microchim. Acta*, 2013, **180**, 493–499.

51 Y. Wei, C. Gao, F. L. Meng, H. Li, L. Wang, J. H. Liu and X. J. Huang, SnO_2/reduced graphene oxide nanocomposite for the simultaneous electrochemical detection of cadmium(II), lead(II), copper(II), and mercury(II): an interesting favorable mutual interference, *J. Phys. Chem. C*, 2012, **116**, 1034–1041.